

Title No. 119-S30

# Modeling of Alkali-Silica Reaction-Affected Shear-Critical Reinforced Concrete Structures

by Anca C. Ferche and Frank J. Vecchio

*Analytical procedures for enhanced nonlinear finite element analysis of shear-critical reinforced concrete structures affected by alkali-silica reaction (ASR) are presented. A novel model that addresses the directional variations in the mechanical properties of ASR-affected concrete is developed; in it, the residual mechanical properties are evaluated based on the sustained long-term stress condition and on the severity of the expansion. The proposed model is implemented within a nonlinear finite element analysis program and validation analyses are carried out to examine the accuracy of the methodology proposed, as well as to identify mechanisms that have a significant influence on the analysis of ASR-affected specimens that are prone to brittle failure. It is found that more accurate predictions are obtained when considering directionality in the mechanical properties using the model developed. The results also indicate that for ASR-affected structures in the field, material information from either damaged or undamaged concrete can be used as valuable information for numerical analysis.*

**Keywords:** alkali-silica reaction (ASR); beams; direction-dependent mechanical properties; finite element analysis; panels; shear walls.

## INTRODUCTION

Concrete is one of the most used materials in the world as it continues to be the material of choice in the construction industry. However, concrete is vulnerable to several factors that can cause premature deterioration. The most common and severe forms of deterioration are usually caused by a combination of factors and are linked with the volume expansion of concrete and reinforcing bars. Among these deterioration mechanisms are endogenous chemical reactions such as alkali-silica reactivity (ASR), which lead to expansion and cracking of concrete that in turn may result in cover spalling and corrosion of the embedded reinforcement. As such, structures in need of assessment and advanced modeling are oftentimes existing buildings experiencing different levels of distress.

Population growth together with economic development will exert significant strain on resources. The OECD<sup>1</sup> report on the projection of global material resources estimates that material use will rise from 89 Gt in 2017 to 167 Gt in 2060. This growth will be reflected in all major types of materials. Greenhouse gas emissions are strongly linked to material use policies; today, concrete manufacturing accounts for 9% of the total greenhouse gas emissions, and it is projected that in 2060, 12% of the emissions will be due to concrete production.

The current environmental and economic climate dictates a trend of prudent maintenance, assessment, and rehabilitation of existing structures. Finite element (FE) analyses of

aging and damaged concrete structures that employ rational analytical procedures, with appropriate constitutive models for degradation mechanisms and are capable of analyzing structures under general loading conditions, represent a fundamental research topic for modern structural appraisal.

The work presented in this paper is centered in the realm of macro-modeling, where the emphasis lies on the global behavior of a structure. Therefore, the ASR-induced deformations, stresses, and deterioration of the mechanical properties need to be considered appropriately. There are numerous models in the literature; the majority of them were implemented within the framework of an FE method. The kinetics of the reaction is typically based on experimental studies, while the behavior of concrete is simulated as either linear elastic or nonlinear. Some approaches presented in the literature adopt an elasto-plastic behavior for concrete<sup>2</sup> or a visco-elasto-plastic damage model,<sup>3</sup> while others are based on a smeared fixed crack model.<sup>4,5</sup>

Esposito and Hendriks<sup>6</sup> proposed a classification of the ASR models available in the literature based on the level at which the input and output parameters were defined. The goal of this comprehensive review was to identify models that could be used for structural analysis. A total of 40 modeling approaches were grouped based on concrete expansion, internal pressure, gel production, and ions diffusion-reaction. Apart from the models based on concrete expansion, the other three categories were found to not be directly applicable to the evaluation of the structural response of ASR-affected structures. In addition, the models based on concrete expansion, which have structural assessment as their primary goal, were found to require a large number of input parameters that in many cases were not available. The study concluded that reliable computational modeling of the effects of ASR on the behavior of structures remains an unsolved issue.

The ASCET (Assessment of Structures Subjected to Concrete Pathologies) program was organized by the Canadian Nuclear Safety Commission (CNSC) and by the U.S. Nuclear Regulatory Commission (U.S. NRC) to address aging management of nuclear concrete structures, taking into account the effect of ASR on structural deterioration. As part of the ASCET benchmark exercise, researchers around

*ACI Structural Journal*, V. 119, No. 2, March 2022.

MS No. S-2021-012.R2, doi: 10.14359/51734331, received April 4, 2021, and reviewed under Institute publication policies. Copyright © 2022, American Concrete Institute. All rights reserved, including the making of copies unless permission is obtained from the copyright proprietors. Pertinent discussion including author's closure, if any, will be published ten months from this journal's date if the discussion is received within four months of the paper's print publication.

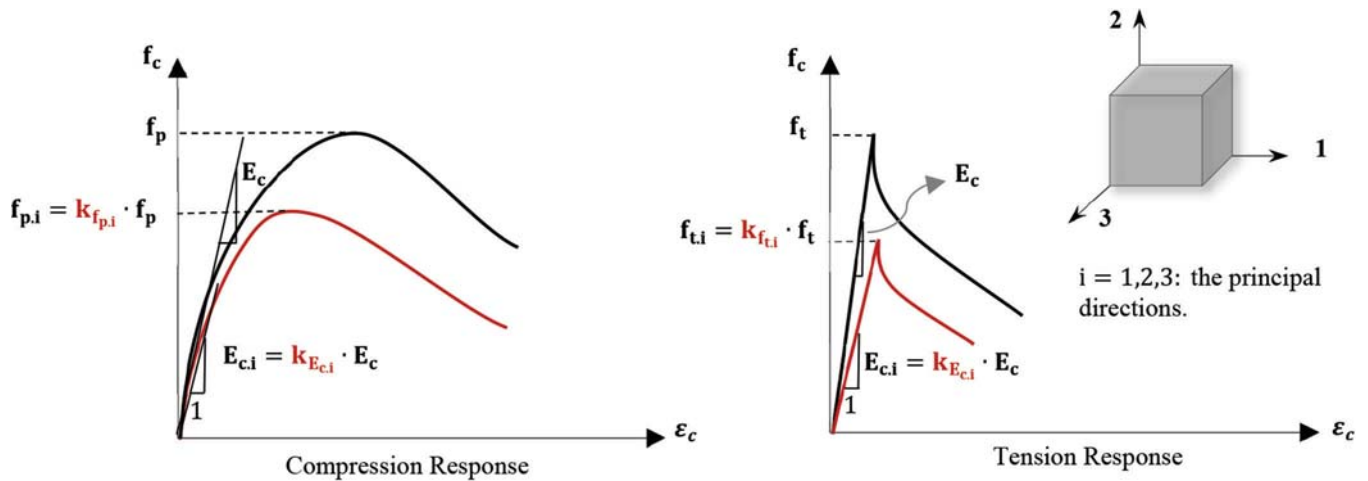


Fig. 1—Modification factors.

the world submitted predictions for the behavior of five shear wall specimens tested at the University of Toronto.<sup>7</sup> Three of these walls experienced various levels of ASR-induced deterioration, and two of them were cast with nonreactive concrete as control specimens. The reports<sup>8,9</sup> of the ASCET workshops summarize the various numerical approaches employed by researchers to model the wall specimens. The modeling techniques varied in terms of the software used, the model type constructed, the concrete and reinforcement models, the ASR expansion model, load application, boundary conditions, and analysis type.

Some of the software programs employed were Abaqus, LS-DYNA, VecTor2, VecTor3, FINAS/STAR, MS ESSI Simulator, or in-house developed software. The concrete models used were alternately based on fracture mechanics, damage plasticity, rigid-body-spring modeling, or smeared crack modeling. ASR-induced expansion was simulated either as equivalent thermal expansion or based on constitutive models for ASR expansion available in the literature. Some researchers found that the boundary conditions of the walls' base blocks had a significant role on the computed response, whereas others found them to have a marginal effect. There was also variability in the representation of the boundary conditions of the top beam, with some researchers allowing rotation and others restraining it.

In general, the peak strength of the wall specimens was captured relatively well by all researchers. On the other hand, high variability in the calculated ductility, stiffness, and shape of the hysteresis loops of the reactive walls was found across the predictions submitted. These analytical results were not as closely matched to the experimental values as were the ultimate strengths of the walls.

One of the major conclusions resulting from this benchmark exercise was that macro-modeling of ASR-affected reinforced concrete structures is heavily reliant on multiple influencing behavioral mechanisms, apart from the ASR expansion model employed.

Proper modeling of material mechanical behavior is essential for reliable structural assessment. For conventional linear elastic assessment procedures, the compressive strength, tensile strength, Young's modulus of elasticity, and Poisson's ratio are typically necessary and sufficient to

characterize the concrete material. When a more advanced analysis is required, additional information is needed to describe the concrete behavior. Generally, the complete uniaxial stress-strain behavior has to be defined analytically. Numerous constitutive models have been developed to describe the concrete compression and tension response based on the mechanical properties measured from tests: compressive strength, tensile strength, and Young's modulus of elasticity.<sup>10</sup> These models, however, were developed for sound, undamaged concrete. The cracking caused by chemical reactions such as ASR influences the concrete stress-strain behavior. The degree to which the behavior of reactive concrete differs from nonreactive concrete was found to be influenced by crack plane orientation and severity of expansion.<sup>11-13</sup>

This paper proposes a novel model for the mechanical properties of ASR-affected concrete. Macroscopic modeling at the material level of the anisotropic damage induced by ASR is focused on the concrete compressive strength, tensile strength, and modulus of elasticity. For sound, undamaged concrete, these mechanical properties have an isotropic character. Material tests on ASR-affected concrete, however, have revealed an anisotropy of the mechanical properties dependent on the magnitude of the ASR damage and on the orientation of the ASR-induced crack planes.<sup>12,14</sup> The proposed model addresses the directional variations in the mechanical properties of ASR-affected concrete through reduction functions applied to the concrete compressive strength, tensile strength, and modulus of elasticity (Fig. 1).

The model was implemented within the algorithms of the nonlinear FE analysis program VecTor2,<sup>10,15</sup> and validation studies were performed on ASR-affected specimens. The reinforced concrete elements examined included panel specimens,<sup>16</sup> shear wall specimens tested by Habibi et al.,<sup>7</sup> and shear-critical beams tested by Deschenes et al.<sup>17</sup>

The validation studies performed on the behavior of ASR-affected specimens were focused on specimens susceptible to brittle failure mechanisms. Sensitivity analyses were also conducted to identify mechanisms that have a significant influence on the computed responses. Specimens tested in the literature that experienced ductile failure were investigated elsewhere.<sup>17,18</sup>

## RESEARCH SIGNIFICANCE

In structures suffering from ASR, the level of expansion and the direction of the ASR-induced crack planes are influenced by the reactivity of the aggregate and by the sustained three-dimensional stress state. In the majority of structures in the field, concrete is experiencing different levels of long-term stress along different directions; as a result, ASR-induced deterioration of concrete mechanical properties is direction-dependent. The model proposed herein addresses the anisotropy of the ASR-affected concrete mechanical properties. The comprehensive analyses of ASR-affected shear-critical reinforced concrete elements provide a novel understanding of the implications of the direction-dependent concrete mechanical properties on the structural response.

## MODELING APPROACH

A two-phased analysis procedure was previously developed for the assessment of ASR-affected structures using nonlinear FE analysis.<sup>18,19</sup> The procedure was incorporated within the program VecTor2,<sup>10,15</sup> which employs a smeared, rotating crack model for concrete behavior.<sup>20</sup> The first phase of the procedure involves the ASR analysis, which differentiates and evaluates two different mechanisms: the deterioration of the concrete mechanical properties, and the ASR-induced strains and stresses developed under long-term loading. Using the results obtained from the first phase, an analysis is then performed to estimate the response of the structure to externally applied short-term loads.

The linear unrestrained ASR expansion, needed for the ASR analysis, can either be input by the user or calculated with one of the two models implemented that include a kinetics component. The ASR-induced strains are evaluated along the principal directions and are carried through the analysis as strain offsets. These expansions are influenced by the stress conditions and so, in this phase of the analysis, the loads applied to the structure should be sustained long-term loads only. For the changes in the concrete mechanical properties, two isotropic options were made available: user-defined properties, or properties calculated based on the recommendations made by the Institution of Structural Engineers,<sup>11</sup> depending on the free expansion and the undamaged concrete strength at 28 days. The mechanical properties of concrete were, therefore, assumed to be uniform in all directions.

Two additional options regarding the mechanical properties of ASR-affected concrete were subsequently implemented as part of this work: the anisotropic formulation of the model described in what follows and its corresponding simplified isotropic version.

### Model formulation

In the model proposed herein, anisotropy in the mechanical properties of concrete is quantified as a function of the reactivity potential of the aggregate and the long-term stress state. Modification factors are determined along each principal direction for the concrete compressive strength  $k_{f_p,i}$ , tensile strength  $k_{f_t,i}$ , and modulus of elasticity  $k_{E_c,i}$  ( $i = 1, 2, 3$  represents the principal direction where  $f_3 < f_2 < f_1$ ). It is worth emphasizing that the modification factors in one

direction are, in part, influenced by the strain and stress states along the other two orthogonal directions. Therefore, distinction is made between stress-free, uniaxial, biaxial, and triaxial stress states. The modification factors are applied to the concrete compressive strength, tensile strength, and modulus of elasticity (Fig. 1) as determined from sound concrete with no ASR-induced damage. For a field structure, these values can be determined from material tests on cores extracted from an undamaged part of the structure. When this is not feasible, an estimation can be made based on the specified strength at 28 days and the age of the structure.

A database was compiled with material test results for ASR-affected concrete, centered on the experiments conducted by Ferche and Vecchio.<sup>14</sup> The majority of the tests reported in the literature were performed on plain concrete specimens, conditioned in an unrestrained state, that developed randomly oriented cracks forming a map-cracking pattern. Although this type of test cannot be used to investigate directional variations in the mechanical properties, they serve an important role for evaluating the effect varying levels of ASR-induced damage have on the concrete mechanical properties. The compiled results, presented in tabular form in Appendix A\* (Tables A.1, A.2, A.3, and A.4), are categorized based on the stress state during the conditioning period, the ASR-induced expansion, and the testing direction relative to the long-term stresses. All the experimental studies compiled contained control specimens cast with nonreactive aggregate against which the behavior of the reactive concrete was compared.

The modification factors  $k_{f_p,i}$ ,  $k_{f_t,i}$ , and  $k_{E_c,i}$ , determined from the compiled database, were defined for the concrete compressive strength, tensile strength, and modulus of elasticity as per Eq. (1), (2), and (3). These factors essentially represent the ratio of the mechanical properties of the reactive concrete to the mechanical properties measured on the nonreactive concrete, normalized to the initial difference measured at 28 days.

For the cases when tension tests were not performed at 28 days, the square root of the ratios of the compressive strengths were used to normalize the tensile tests results (Eq. (2)).

$$k_{f_p,i} = \frac{f_{p,Ri} / f_{p,N}}{f'_{c,Ri} / f'_{c,N}} \quad (1)$$

$$k_{f_t,i} = \frac{f_{t,Ri} / f_{t,N}}{f_{t,Ri,28} / f_{sp,N,28}} \quad (a) \quad \text{or} \quad k_{f_t,i} = \frac{f_{t,Ri} / f_{t,N}}{\sqrt{f'_{c,Ri} / f'_{c,N}}} \quad (b) \quad (2)$$

$$k_{f_t,i} = \frac{E_{c,Ri} / E_{c,N}}{E_{c,Ri,28} / E_{c,N,28}} \quad (3)$$

Note that  $N$  refers to nonreactive concrete;  $R$  to reactive concrete; and  $i$  represents the principal direction ( $i = 1, 2, 3$ , where  $f_3 < f_2 < f_1$ ).

\*The Appendix is available at [www.concrete.org/publications](http://www.concrete.org/publications) in PDF format, appended to the online version of the published paper. It is also available in hard copy from ACI headquarters for a fee equal to the cost of reproduction plus handling at the time of the request.

In the case of unrestrained long-term conditions, the modification factors were defined to represent the lower-bound values from all data points compiled. The proposed modification factors are defined in Eq. (4), (5), and (6) as functions of the linear unrestrained ASR expansion,  $\varepsilon_{ASR}$ . The long-term stress state of uniaxial tension is treated similarly to the unrestrained case in all directions.

$$k_{f_p, free} = \begin{cases} 1.00 - 205.5 \times \varepsilon_{ASR} & \varepsilon_{ASR} \leq 1.8 \times 10^{-3} \\ 0.63 - 1.75 \times \varepsilon_{ASR} & 1.8 \times 10^{-3} < \varepsilon_{ASR} \leq 13.2 \times 10^{-3} \\ 0.75 - 10.9 \times \varepsilon_{ASR} & 13.2 \times 10^{-3} < \varepsilon_{ASR} \leq 27.0 \times 10^{-3} \\ 0.45 & \varepsilon_{ASR} > 27.0 \times 10^{-3} \end{cases} \quad (4)$$

$$k_{E_c, free} = \begin{cases} 1.00 - 344.4 \times \varepsilon_{ASR} & \varepsilon_{ASR} \leq 1.8 \times 10^{-3} \\ 0.42 - 21.9 \times \varepsilon_{ASR} & 1.8 \times 10^{-3} < \varepsilon_{ASR} \leq 13.2 \times 10^{-3} \\ 0.19 - 4.35 \times \varepsilon_{ASR} & 13.2 \times 10^{-3} < \varepsilon_{ASR} \leq 27.0 \times 10^{-3} \\ 0.07 & \varepsilon_{ASR} > 27.0 \times 10^{-3} \end{cases} \quad (5)$$

$$k_{f_t, free} = \begin{cases} 1.00 - 475.9 \times \varepsilon_{ASR} & \varepsilon_{ASR} \leq 0.6 \times 10^{-3} \\ 0.77 - 86.8 \times \varepsilon_{ASR} & 0.6 \times 10^{-3} < \varepsilon_{ASR} \leq 2.5 \times 10^{-3} \\ 0.70 - 60.0 \times \varepsilon_{ASR} & 2.5 \times 10^{-3} < \varepsilon_{ASR} \leq 5.0 \times 10^{-3} \\ 0.40 & \varepsilon_{ASR} > 5.0 \times 10^{-3} \end{cases} \quad (6)$$

Shown in Appendix A, Fig. A.1, are the proposed relationships plotted versus the individual data points. The lower bounds proposed by the Institution of Structural Engineers<sup>11</sup> in 1992 are also plotted. In general, the modification factors decrease as the ASR expansion increases. However, for the same level of expansion, a rather significant scatter in the experimentally determined modification factors can be seen. For the unrestrained case, good agreement can be seen between the proposed relationships and the ISE reduction functions, although they were derived from different specimen databases.

In most instances, however, the concrete component in a structure will experience sustained loading. In the case of a long-term compressive stress state, a distinction is made between the restrained and unrestrained directions. The modification factors along the restrained directions are a function of the stress-free modification factors ( $k_{f_p, free}$ ,  $k_{E_c, free}$ , and  $k_{f_t, free}$ ) defined by Eq. (4), (5), and (6), and the ratio of the linear unrestrained ASR expansion to the elementary strain  $\varepsilon_{ASR}/e_i(f_i)$ . The elementary strain  $e_i(f_i)$  in the principal direction  $i$  is calculated as per Eq. (7). The proposed relationships for the modification factors are applicable to compressive stresses higher than 0.3 MPa (44 psi). This value was chosen based on available experimental data on the development of ASR expansion as a function of the compressive stress.<sup>21</sup> Compressive stresses lower than 0.3 MPa (44 psi) were found not to influence the level of expansion. As such,

compressive stresses lower than 0.3 MPa (44 psi) are treated essentially as a stress-free case.

The elementary strain  $e_i(f_i)$  is calculated as

$$e_i(f_i) = f_i/E_c \quad (7)$$

where  $f_i$  is the long-term compressive stress, along principal direction  $i$  ( $i = 1, 2, 3$ ); and  $E_c$  is the concrete modulus of elasticity of sound concrete at the current age of the structure.

Note that for the elementary strain,  $e_i(f_i)$ , the label  $e$  was chosen as opposed to the customary label for strain  $\varepsilon$ . This choice was made to emphasize that in calculating the elementary strain, the modulus of elasticity corresponding to sound, unaffected concrete is used, assuming linear behavior.

The mechanical properties degradation function proposed for the compressed directions,  $k_{j,i}(f_i)$ , is given in Eq. (8)

$$k_{j,i}(f_i) = k_{j,i, free} + \frac{1}{1.05 \cdot \left( -\frac{\varepsilon_{ASR}}{e_i(f_i)} \right)^{0.09}} - \frac{1}{1.05 \cdot \left( -\frac{\varepsilon_{ASR}}{e_i(0)} \right)^{0.09}} \quad (8)$$

where  $i = 1, 2, 3$  represents the principal directions, where  $f_3 < f_2 < f_1$  (compression negative);  $j = f_p, E_c, f_t$ ;  $f_i$  is the long-term compressive stress along the principal direction  $i$ ;  $k_{j, free}$  is the modification factor evaluated assuming unrestrained stress conditions, according to Eq. (4), (5), and (6);  $\varepsilon_{ASR}$  is the unrestrained linear ASR expansion;  $e_i(f_i)$  is the elementary strain in the principal direction  $i$ , corresponding to the long-term compressive stress  $f_i$ ; and  $e_i(0)$  is the elementary strain in the principal direction  $i$ , corresponding to a compressive stress of 0.3 MPa (44 psi).

To illustrate the relationship between the modification factors  $k_{f_p}$ ,  $k_{E_c}$ ,  $k_{f_t}$ , and the long-term compressive stress  $f_i$ , Fig. 2 provides plots of the compressive stress for two levels of ASR expansion:  $0.5 \times 10^{-3}$  and  $2.0 \times 10^{-3}$ , and a modulus of elasticity of concrete equal to 25,000 MPa (3625 ksi). Constant modification factors were calculated up to a compressive stress level of 0.3 MPa (44 psi) based on the relationships proposed in Eq. (4), (5), and (6), similar to a stress-free condition. For levels of compressive stress larger than 0.3 MPa (44 psi), the modification factors increased with the increase in stress, reflecting the beneficial effect of compressive stresses to counteract the ASR-induced deterioration. The most affected mechanical property was the tensile strength, followed by the modulus of elasticity, and lastly by the compressive strength for both levels of ASR expansion.

In Appendix A, Fig. A.2, ratios of the ASR strain to the elementary strain,  $\varepsilon_{ASR}/e_i(f_i)$ , are plotted with respect to the long-term compressive stress  $f_i$  for various levels of ASR expansion, assuming a modulus of elasticity of concrete equal to 25,000 MPa (3625 ksi). Due to the nature of Eq. (8), an increase in the strain ratio,  $\varepsilon_{ASR}/e_i(f_i)$  corresponds to a decrease in the calculated modification factors, which translates to a more pronounced degradation of the mechanical properties. For the same level of long-term stress  $f_i$ , the strain ratio  $\varepsilon_{ASR}/e_i(f_i)$  increases with the increase in ASR strain

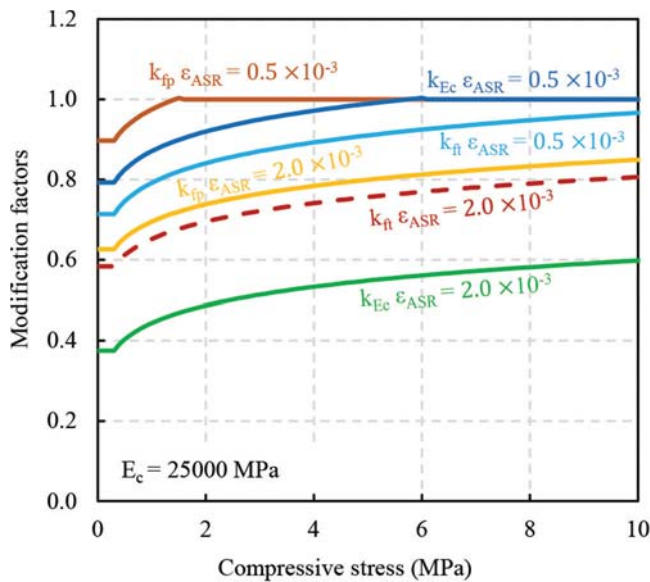


Fig. 2—Modification factors versus long-term compressive stress for  $E_c = 25,000$  MPa. (Note:  $E_c = 25,000$  MPa was chosen for illustrative purposes only. The model is not limited to this value for  $E_c$ . 1 MPa = 145 psi.)

(Fig. A.2), or with the increase in the undamaged modulus of elasticity.

The decision behind establishing this relationship between the modification factors, the ASR-induced strain, and the undamaged modulus of elasticity of concrete was made based on empirical observations. A higher ASR-induced expansion usually led to a more pronounced degradation of mechanical properties. Due to the ability of a more porous concrete matrix to accommodate the expansive ASR gel before sufficient pressure develops to cause cracking, concrete with reduced porosity was found to be more severely affected by ASR deleterious effects compared to concrete with higher porosity levels.<sup>22-24</sup> Porosity is strongly associated with the modulus of elasticity of concrete; a reduced porosity generally results in a higher modulus of elasticity when the same components are used in the mixture design.<sup>25</sup> As the concrete porosity is a property that in the majority of cases is not as readily available as the modulus of elasticity, it was decided to use the modulus of elasticity as an indicator of the porosity level, thus influencing the calculated modification factors.

The modification factors are applied to the unaffected mechanical properties of concrete as such

$$f_{p,i} = k_{f_{p,i}} \cdot f_p \quad (9)$$

$$E_{c,i} = k_{E_{c,i}} \cdot E_c \quad (10)$$

$$f_{t,i} = k_{f_{t,i}} \cdot f_t \quad (11)$$

where  $i = 1, 2, 3$  represents the principal directions, where  $f_3 < f_2 < f_1$ .

Appendix A contains Tables A.1, A.2, A.3, and A.4 summarizing the calculated modification factors versus the

experimental measured results for the specimens that were part of the compiled database. The tables summarize: the levels of unrestrained linear ASR expansion  $\epsilon_{ASR}$ ; the long-term conditioning stress state; the testing direction relative to the long-term stresses; the measured mechanical properties (compressive strength  $f_p$ , modulus of elasticity  $E_c$ , and tensile strength  $f_t$ ); the experimentally determined modification factors for the mechanical properties,  $k_{j,exp}$ ; the calculated modification factors,  $k_{j,calc}$ ; and the ratios of calculated to experimental values for the modification factors. The index  $j$  represents the mechanical property under consideration ( $j = f_p, E_c, f_t$ ). A wide variance of the experimental modification factors is observed for similar expansion levels. As such, the adopted model was chosen to be conservative, reflected in the mean of the ratios of calculated to experimental values for the modification factors.

For analytical procedures that cannot accommodate anisotropic implementation for the mechanical properties of concrete, an isotropic version is proposed, using the average modification factors. Therefore, the isotropic model applies the average modification factors calculated along each principal direction to the corresponding mechanical properties, as shown in Eq. (12), (13), and (14).

$$f_{p, isotropic} = \frac{(k_{f_{p,1}} + k_{f_{p,2}} + k_{f_{p,3}})}{3} \cdot f_p \quad (12)$$

$$E_{c, isotropic} = \frac{(k_{E_{c,1}} + k_{E_{c,2}} + k_{E_{c,3}})}{3} \cdot E_c \quad (13)$$

$$f_{t, isotropic} = \frac{(k_{f_{t,1}} + k_{f_{t,2}} + k_{f_{t,3}})}{3} \cdot f_t \quad (14)$$

### Finite element implementation

To implement the proposed model for the mechanical properties of ASR-affected concrete, an iterative solution algorithm is required due to the interdependency of the ASR-induced strains, the stress state, and the mechanical properties. Such was done within the algorithms of nonlinear FE analysis program VecTor2 in two forms: an anisotropic implementation with directional-dependency of the mechanical properties, and an isotropic implementation, independent of the orientation of the principal stress field. The FE implementation for a two-dimensional approach is summarized in what follows.

The anisotropic model for the mechanical properties of concrete consists of evaluating modification factors for the compressive strength, modulus of elasticity, and the tensile strength along each principal direction. The modification factors are calculated based on Eq. (4), (5), (6), and (8) in an iterative process and are applied to the undamaged mechanical properties according to Eq. (9), (10), and (11).

Upon the completion of the ASR analysis, in the second stage of the analysis, the modification factors are reevaluated at each step as the orientation of the principal stress field changes from the initial orientation.

**Table 1—Panel specimen properties and test results**

ID	$\rho_x$ , %	$\rho_y$ , %	$\rho_z$ , %	$f_{cp}$ , MPa	$E_c$ , MPa	$v_{cr}$ , MPa	$\gamma_{cr} \times 10^{-3}$	$v_u$ , MPa	$\gamma_u \times 10^{-3}$	$\epsilon_{ASR} \times 10^{-3}$ Reactive aggregate
AF1	3.31	0.42	—	57.2	33,700	2.19	0.24	6.75	9.59	0.12*
AF2	3.31	0.84	—	58.4	33,500	2.74	0.32	8.64†	6.54†	Nonreactive
AF3	3.31	0.42	—	38.2	18,300	4.34	0.53	6.99	6.50	2.32
AF4	3.31	0.84	—	41.3	18,600	4.32	0.35	9.77	7.37	Jobe-Newman
AF5	3.31	0.42	—	52.5	21,000	3.96	0.33	6.99	6.67	1.23
AF6	3.31	0.84	—	52.1	20,100	4.32	0.49	9.63	7.39	Spratt
AF7	3.31	0.42	1.69	46.3	21,200	4.90	0.50	7.33	7.07	2.49
AF8	3.31	0.84	1.69	47.1	19,400	5.67	0.87	10.42	7.83	Jobe-Newman
AF9	3.31	0.20	—	46.9	18,900	3.90	0.25	4.79	3.81	2.36
AF10	3.31	1.66	—	50.9	21,200	5.21	0.48	10.79‡	5.98	Jobe-Newman

\*Expansion primarily attributed to swelling due to water absorption.

†Edge failure.

‡Tested under cyclic loading.

Note: 1 MPa = 145 psi.

As such,  $k_{ASR,i}$ ,  $l_{ASR,i}$ , and  $m_{ASR,i}$  are defined as the direction cosines for the orientation of the principal stress field with respect to the global reference axes at the end of the ASR analysis;  $i = 1, 2, 3$  represent the principal directions where  $f_3 < f_2 < f_1$  (compression negative). Similarly, the direction cosines  $k_i$ ,  $l_i$ , and  $m_i$  are defined for the current orientation of the principal stress field with respect to the global reference axes;  $i = 1, 2, 3$  represent the principal directions where  $f_3 < f_2 < f_1$  (compression negative).

For two-dimensional analyses, the modification factors corresponding to the current first and second in-plane principal directions,  $k_{j,1c}$  and  $k_{j,2c}$  ( $j = f_p, E_c, f_i$ ), are evaluated as

$$k_{j,1c} = \sqrt{\frac{k_{j,1}(k_1 k_{ASR,1} + l_1 l_{ASR,1} + m_1 m_{ASR,1})^2 + k_{j,2}(k_2 k_{ASR,2} + l_2 l_{ASR,2} + m_2 m_{ASR,2})^2 + k_{j,3}(k_3 k_{ASR,3} + l_3 l_{ASR,3} + m_3 m_{ASR,3})^2}{k_{j,1}^2 + k_{j,2}^2 + k_{j,3}^2}} \quad (15)$$

$$k_{j,2c} = \sqrt{\frac{k_{j,1}(k_2 k_{ASR,1} + l_2 l_{ASR,1} + m_2 m_{ASR,1})^2 + k_{j,2}(k_2 k_{ASR,2} + l_2 l_{ASR,2} + m_2 m_{ASR,2})^2 + k_{j,3}(k_2 k_{ASR,3} + l_2 l_{ASR,3} + m_2 m_{ASR,3})^2}{k_{j,1}^2 + k_{j,2}^2 + k_{j,3}^2}} \quad (16)$$

where  $k_{j,1}$ ,  $k_{j,2}$ , and  $k_{j,3}$  are the modification factors calculated along the principal directions at the end of the ASR analysis, considering long-term sustained loading conditions only, according to the model proposed.

For a two-dimensional analysis procedure, the modification factors calculated in the out-of-plane direction remain constant throughout the analysis, and  $m_1 = m_2 = 0.0$ .

Given in Appendix B is the nonlinear analysis algorithm employed in VecTor2. Highlighted with red are the steps where ASR strains are calculated and included in the concrete prestrains vector,  $\{\epsilon_c^o\}$ , and where the mechanical properties modification factors are evaluated.

Validation studies were performed on ASR-affected specimens to obtain an indication of the accuracy of the proposed model. All the analyses were performed with the version of

VecTor2 dated November 2019, and were constructed with VecTor2's pre-processor software, FormWorks 4.3.<sup>15</sup> The post-processor Augustus<sup>26</sup> was used to process and visualize the results.

### PANEL ELEMENTS

A set of 10 reinforced concrete panel elements tested by Ferche and Vecchio<sup>16</sup> were investigated as part of the validation studies. The panels, 890 mm (35 in.) square x 70 mm (2.7 in.) thick, contained varying amounts of in-plane and out-of-plane reinforcement, and were cast with either nonreactive, reactive fine (Jobe-Newman), or reactive coarse (Spratt) aggregate. The specimens were conditioned under elevated humidity and temperature to accelerate the reaction rate. At the end of the conditioning period, the panels were tested under in-plane pure shear loading conditions. The following properties and test results are shown in Table 1 for the panel specimens: the reinforcement ratios  $\rho_x$ ,  $\rho_y$ , and  $\rho_z$ ; the concrete compressive strength and modulus of elasticity  $f_{cp}$  and  $E_c$ ; shear stress and strain at cracking  $v_{cr}$  and  $\gamma_{cr}$ ; ultimate stress and strain  $v_u$  and  $\gamma_u$ ; the ASR expansion measured on accompanying prisms specimens  $\epsilon_{ASR}$ ; as well as the type of reactive aggregate used in the mixture.

Each panel was modeled as a single four-node plane stress rectangular element. The analyses were performed in force-controlled conditions. The shear stress was increased by 0.10 MPa (14.5 psi) at each analysis step for the monotonically tested panels and by 0.20 MPa (29 psi) for the cyclically loaded panel. The reinforcement was modeled as smeared reinforcement with the mechanical properties measured from coupon tests, summarized in Table C.1 of Appendix C. Also summarized in Appendix C are the concrete and reinforcement stresses at the end of the conditioning period, before the beginning of the shear test (Table C.2). The concrete compressive stresses in the x-direction varied between 3.74 and 6.06 MPa (542 and 879 psi), while in the y-direction they were in the 0.89 to 3.33 MPa (129 to 483 psi) interval, depending on the reactivity of the mixture and

the reinforcement ratios provided. The x-direction reinforcement had stresses ranging from 86 to 183 MPa (12.4 to 26.5 ksi), while the y-direction reinforcement reached stresses between 201 and 444 MPa (29.2 and 64.4 ksi). Perfect bond was assumed between concrete and reinforcement.

For the nonreactive panels, the concrete properties specified were the concrete compressive strength and the modulus of elasticity, as measured from the cylinders at test day. For the ASR-affected panels, three different cases were considered in terms of the concrete properties:

1. Using the concrete compressive strength as measured from reactive cylinders at test day that were cast and conditioned with the reactive panels, employing no degradation functions for the mechanical properties of concrete—labeled Cylinder.

2. Using the concrete compressive strength as measured from nonreactive cylinders at test day that were cast with the control panels, together with the anisotropic model for degradation of mechanical properties proposed—labeled Anisotropic.

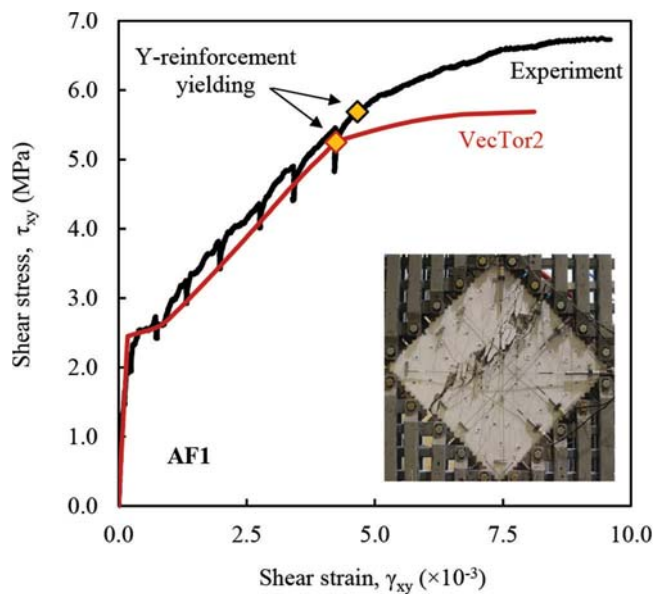
3. Using the concrete compressive strength as measured from nonreactive cylinders at test day that were cast with the control panels, together with the isotropic model for degradation of mechanical properties proposed—labeled Isotropic.

Two ASR-induced strain calculation models, the Charlwood et al.<sup>21</sup> model and the Saouma and Perotti<sup>27</sup> model, were investigated to quantify the influence of ASR strain calculation on the analytical response. The Charlwood model calculates ASR expansion as a function of the compressive stresses and treats each principal direction independently. The Saouma and Perotti model assumes ASR expansion is volumetrically distributed and that expansions in the three principal directions are interdependent. Thus, for each of the three cases considered in terms of concrete properties, two analyses were performed based on the ASR expansion model: one using the Charlwood model and the other one using the Saouma and Perotti model.

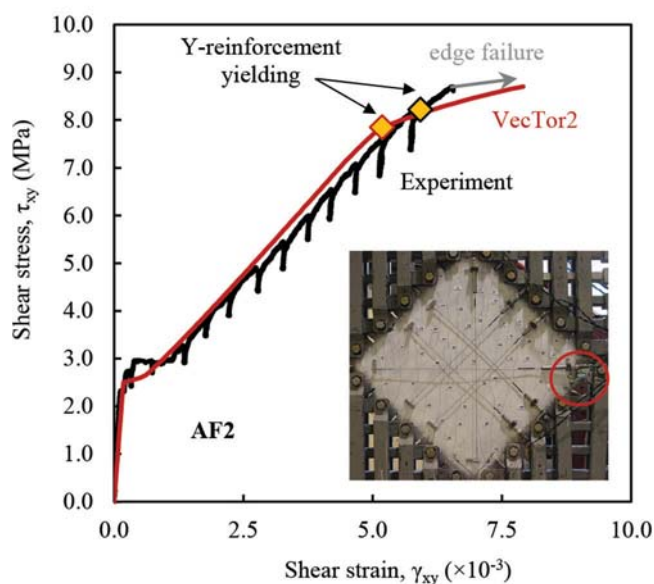
In addition, for each reactive panel, an analysis was performed neglecting the effect of ASR-induced expansion and using the concrete mechanical properties as determined from the reactive cylinders test. This analysis was performed as it is similar to the approach taken by several researchers when estimating the strength of field ASR-affected structures.<sup>28-30</sup>

Prior to modeling the ASR-affected specimens, the accuracy of VecTor2 in predicting the response of the nonreactive control panels was investigated. The FE analysis results for the nonreactive panels AF1 and AF2 are shown in Fig. 3 in comparison to the experimentally measured responses. The numerical results were reasonably similar to the experimental findings. Analytically, the failure mechanism was initiated by the yielding of the reinforcement in the Y-direction for both nonreactive panels. This was consistent with the experimental observations.

Panel AF1 exhibited higher shear stiffness upon yielding of the y-direction reinforcement compared to the numerical model, as shown in Fig. 3(a). A similar observation was previously noted by Luo<sup>31</sup> and Carnovale<sup>32</sup> on similar



(a) Panel AF1



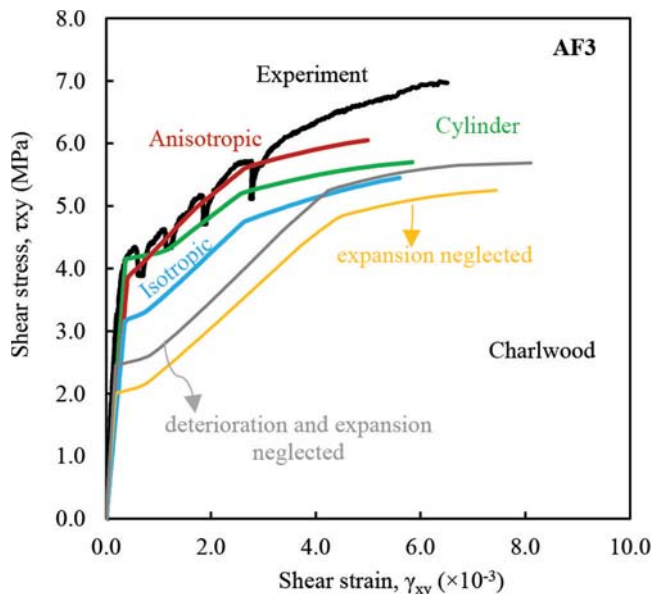
(b) Panel AF2

Fig. 3—Numerical versus experimental response for nonreactive panel specimens. (Note: 1 MPa = 145 psi.)

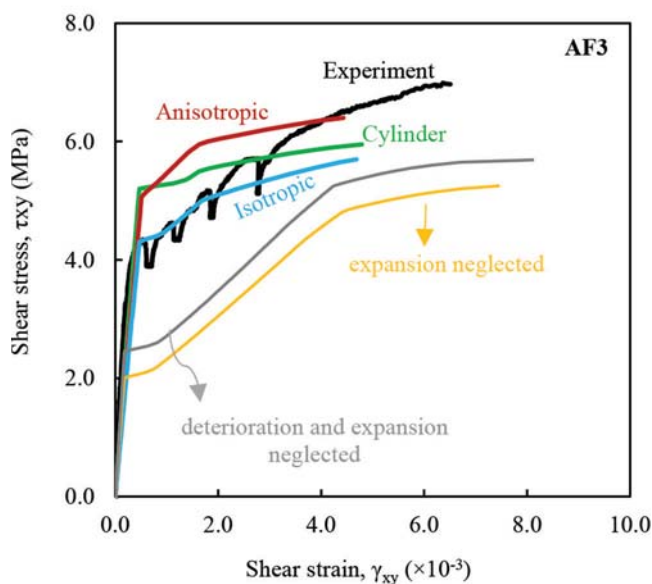
panels. Panel AF2 suffered an edge failure soon after the y-direction reinforcement started yielding. Numerically, the failure shear stress and strain predicted were close to the ultimate shear stress and strain measured experimentally, illustrated in Fig. 3(b). It should be pointed out that the reinforcement was cold-formed and did not have a well-defined yield plateau, which contributed to the discrepancy in the analysis results.

### Panel AF3

The analysis of representative reactive Panel AF3 is discussed in what follows. Table C.3 presents the stress and strain state of the panel, upon the completion of the ASR conditioning period, at the end of each of the various ASR analyses undertaken. Thus, Table C.3 summarizes



(a) Panel AF3 – Charlwood model for expansion



(b) Panel AF3 – Saouma and Perotti model for expansion

Fig. 4—Numerical versus experimental response for Panel AF3. (Note: 1 MPa = 145 psi.)

the concrete stresses  $f_{cx}$  and  $f_{cy}$ , the total strains  $\epsilon_{x,\text{total}}$  and  $\epsilon_{y,\text{total}}$ , and the concrete strains  $\epsilon_{x,\text{ASR}}$  and  $\epsilon_{y,\text{ASR}}$  in the x- and y-directions. The reported measured strains and stresses were based on measurements of total surface strains using Zurich gauges. The data show that the ASR expansion model influenced the calculated initial stress and strain state significantly, compared to the approach taken to model the mechanical properties, which had a marginal effect. In this case, the Saouma and Perotti (labeled S&P) predictions for the ASR-induced strains matched the experimental measurements to a closer degree than did the Charlwood model. As expected, neglecting the ASR expansion resulted in no initial strains and stresses for the panel specimens.

Shown in Fig. 4(a) are the results obtained for Panel AF3 using the Charlwood model for expansion. In terms of the

cracking strength prediction, the Charlwood model was conservative regardless of the approach considered for the concrete mechanical properties. The results obtained with either anisotropic or cylindrical properties closely matched the experimental values, whereas the isotropic model resulted in a lower cracking strength. In terms of overall predicted behavior, the anisotropic model matched more closely the experimental behavior compared to the isotropic model or the one using the cylinder properties. Similar to the control panel, for AF1, upon yielding of the y-direction reinforcement, the calculated response was less stiff compared to the experimental one.

The Saouma and Perotti model, used with either the anisotropic model or with the model considering cylinder properties, overestimated the cracking strength of the panel, as illustrated in Fig. 4(b). This was symptomatic of an overestimation of the ASR-induced prestress. However, the Saouma and Perotti model used with the isotropic model for degradation of concrete mechanical properties matched the experimental cracking strength closely. This was the result of more severe degradation of the mechanical properties predicted by the isotropic model compared to the anisotropic one which, in this case, counteracted better the initial high level of prestress calculated.

The results obtained neglecting the effects of ASR expansion and using the reactive cylinder properties resulted in a significant underestimation of the cracking strength and ultimate capacity. The ultimate shear strain, however, was better predicted (Fig. 4). An additional analysis was carried out for Panel AF3 with both ASR-induced expansion and deterioration neglected. This analysis also underestimated the response compared to the experimental one.

Given in Appendix C in Tables C.4 and C.5 are the modification factors calculated along the principal directions for the initial and final load stages. The modification factors change as the direction of the principal stresses changes, as detailed previously. In-depth analyses of the panel specimens can be found elsewhere.<sup>33</sup>

## Discussion—panel elements

The results are summarized for the monotonically tested reactive panels in Table 2. For each type of analysis performed, the mean and coefficient of variation are shown for the cracking shear stress ratio  $v_{cr,\text{Calc}}/v_{cr,\text{Exp}}$ , the ultimate shear stress ratio  $v_{u,\text{Calc}}/v_{u,\text{Exp}}$ , and the ultimate shear strain ratio  $\gamma_{u,\text{Calc}}/\gamma_{u,\text{Exp}}$ .

The anisotropic mechanical properties model employed with the Charlwood model for ASR expansion yielded superior predictions compared to the rest of the analyses, followed closely by the model using the cylinder properties. The analyses performed with the Saouma and Perotti model overestimate the cracking strength, whereas the ultimate shear strength matched well with the experimental capacity.

Reactive Panel AF10 was subjected to cyclic shear loading. The target peak shear stress of each cycle was 10.8 MPa. The panel failed after 15 cycles. Shown in Table C.6 are the results obtained for each different analysis performed. The cracking strength, post-cracking stiffness, and the number of cycles to failure were better captured using either the

**Table 2—Summary of results: reactive panels\***

ASR expansion model	Mechanical properties	$V_{cr.Calc}/V_{cr.Exp}$		$V_{u.Calc}/V_{u.Exp}$		$\gamma_{u.Calc}/\gamma_{u.Exp}$	
		Mean	COV, %	Mean	COV, %	Mean	COV, %
Charlwood	Anisotropic	0.86	7.82	0.89	4.35	0.87	12.89
	Isotropic	0.74	6.93	0.81	5.83	0.92	17.79
	Cylinder	0.97	6.87	0.86	4.45	0.88	7.60
Saouma and Perotti	Anisotropic	1.19	9.76	0.93	4.77	0.70	17.94
	Isotropic	1.05	10.08	0.84	4.42	0.80	28.65
	Cylinder	1.27	6.86	0.91	6.44	0.76	8.79
Neglected	Cylinder	0.50	13.40	0.80	5.37	1.12	9.82

\*Includes Panels AF3, AF4, AF5, AF6, AF7, AF8, and AF9.

proposed anisotropic model or the reactive cylinder properties together with the Charlwood model for expansion.

The following trends can be identified following the analytical investigation of the ASR-affected panels:

1. The Charlwood model for evaluating ASR-induced strains produced results that better matched the experimental behavior of the panels (cracking strength, post-cracking stiffness, post-yielding stiffness, ultimate capacity) compared to the Saouma and Perotti model.

2. The influence of the model for the concrete mechanical properties on the evaluation of ASR-induced strains was significantly smaller compared to the influence of the ASR expansion model. This was found to be true regardless of the level of ASR expansion or the reinforcement ratios.

3. The Saouma and Perotti model evaluated higher ASR-induced strains compared to the Charlwood model. For the biaxially reinforced panels, the strains calculated with the Saouma and Perotti model were closer to the experimental measurements, while for the triaxially reinforced panels AF7 and AF8, the Charlwood model resulted in better predictions.

4. The proposed anisotropic model for the mechanical properties of concrete resulted in the most accurate predictions of the overall response of the panels.

5. The isotropic model calculated more severe degradation parameters for the concrete compressive strength, tensile strength, and modulus of elasticity compared to the anisotropic model in the first and second principal directions. This resulted in more conservative predictions.

6. The isotropic model yielded more conservative results in comparison to the model employing cylinder concrete properties as well.

7. For all panels, neglecting the ASR expansion resulted in significant underestimations of the cracking strength and ultimate shear stress.

### SHEAR WALLS

To gauge the reliability of the model for the analysis of elements with common structural applications, the shear walls tested by Habibi et al.<sup>7</sup> were examined. All shear walls were similar in terms of reinforcement details, geometric dimensions, and configuration, as shown in Fig. 5. The specimens had a barbell-shaped cross section and were built integrally with rigid top and bottom beams. The height of the shear walls, from the top of the bottom slab to the soffit of

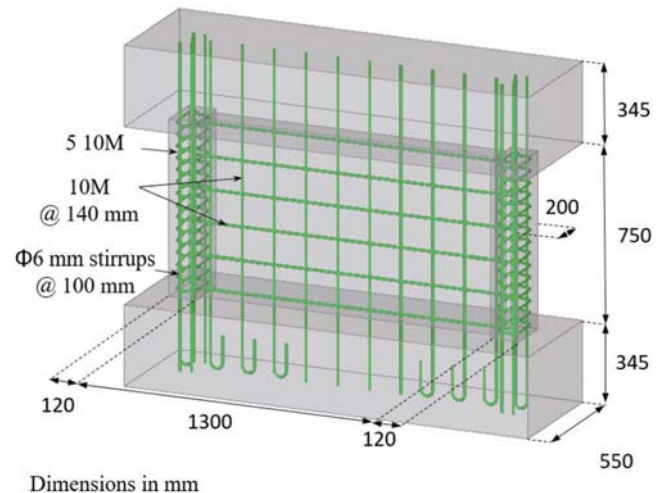


Fig. 5—Geometric details and reinforcement layout of shear wall specimens. (Note: 1 mm = 0.04 in.)

the top slab, was 750 mm (29.5 in.). The web was 100 mm (4 in.) thick and 1300 mm (51.1 in.) wide. The boundary elements had a thickness of 200 mm (7.8 in.) and a width of 120 mm (4.7 in.). In the web region, the horizontal reinforcement ratio was 0.80%, and the vertical reinforcement ratio was 0.77%. The flanges had 2.10% reinforcement ratio in the vertical direction, 0.67% in the horizontal direction, and 0.44% in the out-of-plane direction.

Two specimens were cast with nonreactive concrete—REG A and REG B walls; three specimens—ASR A1, ASR B1, and ASR B2 were cast with reactive Spratt aggregate. The concrete compressive strength  $f_{cp}$  and modulus of elasticity  $E_c$ , as determined from standard 100 mm (4 in.)  $\Phi$  cylinders on the test day, are shown in Table 3. For the reactive specimens, the free expansions ( $\epsilon_{ASR}$ ), determined from expansion prisms, were used as input for the ASR analyses.

Sensitivity studies were carried out to identify the mechanisms that play a significant role in the computed responses of these walls. The FE models had different levels of complexity to address the parameters investigated. A predictive approach was adopted, underlying the steps commonly required for a blind prediction exercise or for structural appraisal. The sensitivity studies were classified into three categories: modeling details, behavioral mechanisms, and material response. In-depth analyses of the sensitivity studies are reported elsewhere.<sup>33</sup>

**Table 3—Shear wall specimens: concrete properties and summary of results**

ID	$f_{cp}$ , MPa	$E_c$ , MPa	$\epsilon_{ASR}$ , $\times 10^{-3}$	$P_{u,Calc}$ , kN	$P_{u,Exp}$ , kN	$\delta_{u,Calc}$ , mm	$\delta_{u,Exp}$ , mm	$P_{u,Calc}/P_{u,Exp}$	$\delta_{u,Calc}/\delta_{u,Exp}$
REG A	79.0	47,150	0.33*	1172	1180	7.00	6.10	0.99	1.15
REG B	80.1	46,650	0.33*	1178	1187	7.06	6.30	0.99	1.12
ASR A1	63.7	35,750	1.90	1180	1355	4.50	6.20	0.87	0.73
ASR B1	67.1	32,600	2.15	1205	1240	4.88	4.90	0.97	1.00
ASR B2	63.0	28,100	2.23	1187	1243	4.60	2.60	0.95	1.77
Mean				—				0.96	1.15
COV, %				—				4.72	29.8

\*Expansion primarily attributed to swelling due to water absorption.

Note: 1 kN = 0.225 kip; 1 mm = 0.04 in.

The following set of factors were found to not significantly affect the calculated behavior: smeared versus discrete representation of the reinforcement, three-dimensional effects, bond strength, reinforcement buckling, cover spalling and element erosion, ASR expansion models, nor hysteretic behavior of the concrete. Nevertheless, these aspects may have a crucial effect for specimens with different geometries or failure modes.

Three factors however, were identified as having a notable effect on the computed response: representation of boundary conditions, strength enhancement due to confinement, and concrete compression response. In this respect, the following conclusions can be made:

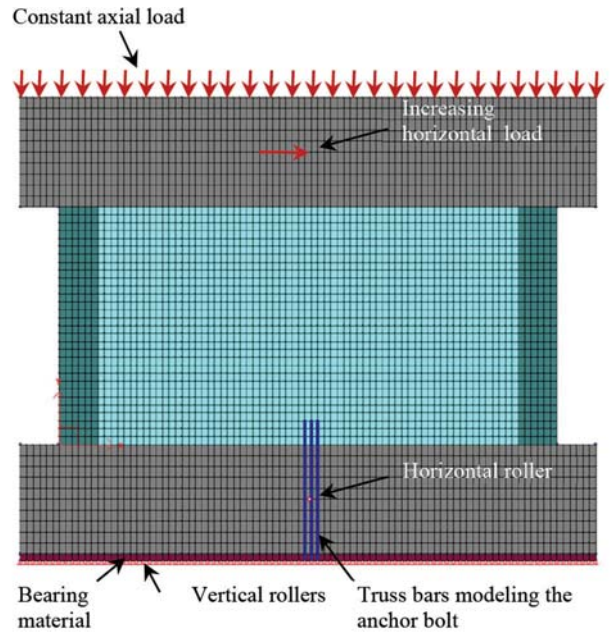
1. The magnitude and direction of the ASR-induced strains depend on internal and external restraints, as well as on long-term loading conditions, all of which must be appropriately considered for the ASR analysis.

2. Confinement conditions exert a significant influence on many aspects of behavior, such as cracking, ultimate load capacity, and post-peak ductility. Modeling of confinement-related mechanisms has to be made in a realistic fashion.

3. The uniaxial concrete compression model impacts the computed ductility appreciably. It is not sufficient to accurately capture the concrete compressive strength and modulus of elasticity. The strain at peak stress and post-peak stiffness need to be properly represented as well.

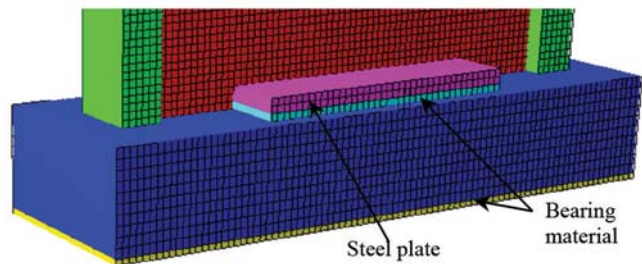
Following the sensitivity study, for the final iteration of analyses, it was decided to adopt an FE model with a 20 mm (0.79 in.) mesh size, illustrated in Fig. 6(a). The wall-floor connection (that is, the anchor bolt assembly) was modeled by defining a layer of bearing material elements beneath the bottom beam that provided stiffness in compression only, thus allowing for potential uplift. The anchor bolt was represented by three truss bars with equivalent cross-sectional area. In addition, as shown in Fig. 6(b), the anchoring steel plate provided at the top of the bottom beam was also modeled using two layers of steel elements and one layer of bearing material to allow free expansion of the wall specimen due to ASR and prevent additional confinement.

The reinforcement was represented as smeared, and the Hoshikuma model was used for concrete in compression; all other behavioral parameters were the default VecTor2 options, as given in Appendix D, Table D.2. For the analyses of the reactive walls, the Charlwood model for



(a) FE model for the shear wall specimens (FormWorks).

Note: the layer of elements representing the steel plate is not shown



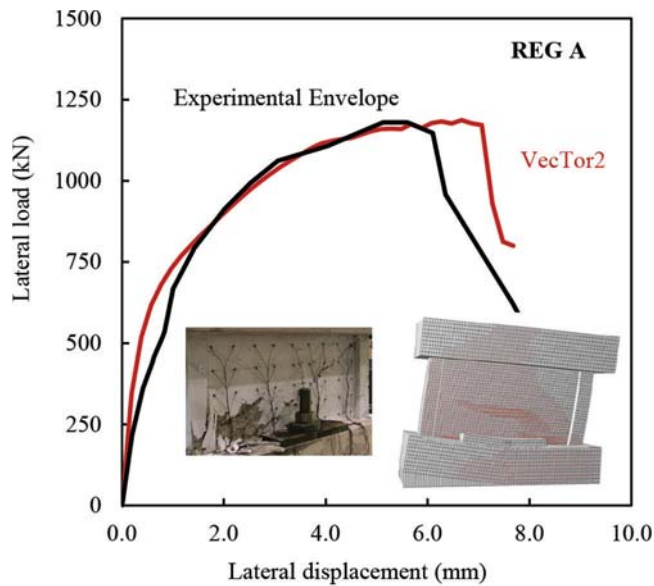
(b) Boundary conditions (Augustus) showing the steel plate.

Note: the truss bars representing the anchor bolt are not shown

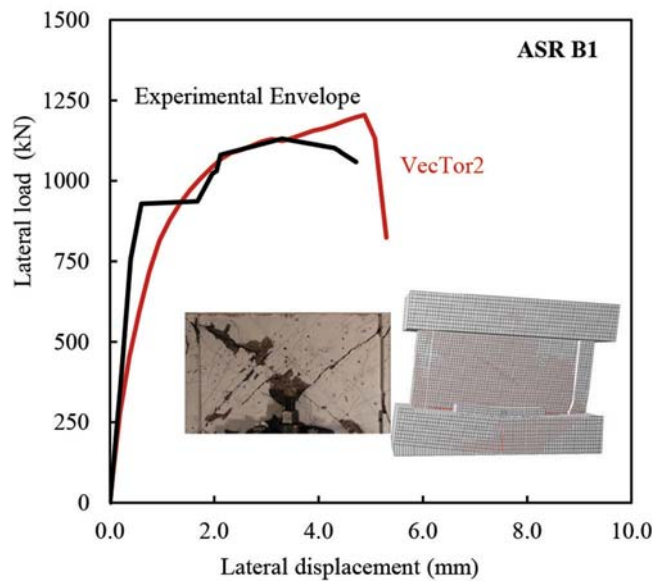
Fig. 6—Finite element model for shear wall specimens.

expansion was used together with the anisotropic model for the mechanical properties of concrete. For the shear wall specimens with experimentally measured unsymmetrical responses, the envelope containing the maximum measured load was selected.

Comparisons between the envelope of the experimental results and the monotonically computed responses are shown in Fig. 7 for nonreactive wall REG A and for the



(a) REG A response



(b) ASR B1 response

Fig. 7—Numerical versus experimental responses for selected shear walls. (Note: 1 kN = 0.225 kip; 1 mm = 0.04 in.)

reactive ASR A1 wall. For both specimens, the initial stiffness, peak load, ductility, and failure mode were captured well by the FE analysis. Shown in Table 3 is the summary of results for all wall specimens in terms of peak force  $P_u$  and ultimate displacement  $\delta_u$  ratios for calculated-to-experimental values. Note that the calculated and experimental ultimate displacements were reported as the displacements recorded before a reduction higher than 15% in the horizontal load was measured. The peak loads of all wall specimens were matched well by the analytical results, with the general tendency for the predictions being on the conservative side. The ultimate displacements were reasonably well captured for the nonreactive walls and for the reactive wall ASR B2; however, for walls ASR A1 and ASR B2, greater dissimilarity was noted between the calculated and the

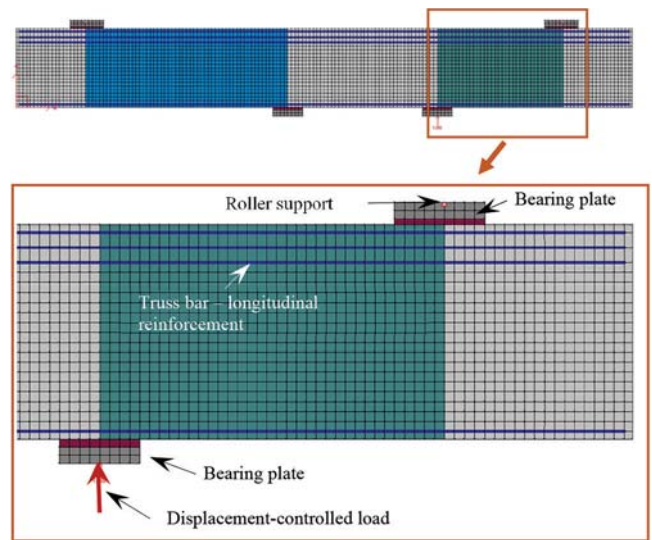


Fig. 8—Finite element model for beam specimens—deep beam test.

measured values. The nonreactive walls developed a failure mode governed by diagonal shear with sliding between the wall and the bottom beam, and the ASR-affected walls failed due to diagonal shear. The numerical analyses captured the appropriate failure modes for all wall specimens.

### SHEAR-CRITICAL BEAMS

The validation analyses examining the proposed model for the mechanical properties of ASR-affected concrete included large shear-critical beam specimens tested by Deschenes et al.<sup>17</sup> The reactive specimens were cast with Jobe-Newman fine aggregate and two nonreactive specimens were used as a basis of comparison for long-term structural performance.

The specimens were structurally identical, with a width of 533 mm (21 in.) and a height of 1067 mm (42 in.). Two independent shear tests, a deep beam shear test and a sectional shear test, were performed on each specimen; one at each end. The shear span-depth ratio was 1.85 for the deep beam tests and 3.0 for the sectional shear tests. The longitudinal reinforcement ratio of 3.1% was chosen such that a shear failure would be obtained. The minimum amount of transverse reinforcement was provided to ensure that the specimens represented the least conservative field scenario: 0.31% for the deep beam tests and 0.15% for the sectional shear tests. The specimens were conditioned outside, with a sustained load applied to simulate long-term service loading.

The FE model constructed to represent these specimens, showing the support conditions and the load application for the deep beam test scenario, is illustrated in Fig. 8. The longitudinal reinforcement was represented using discrete truss bar elements, whereas the stirrups and the crack control reinforcement were smeared within the concrete elements. The mesh size used was 50 x 50 mm (2 x 2 in.). A monotonically increasing displacement-controlled load was applied in increments of 0.25 mm ( $9.8 \times 10^{-3}$  in.) until failure. For the reactive specimens, the load applied during the conditioning phase was introduced as nodal loading active during the ASR analysis only. Additionally, the dead load of the specimens was simulated as gravity loading during both

**Table 4—Shear-critical beams: concrete properties and summary of results**

Specimen	Concrete		$V_{u,Exp}$ , kN	$V_{u,Calc}$ , kN		$V_{u,Calc}/V_{u,Exp}$	
	$f_{cp}$ , MPa	$\epsilon_{ASR}$ , $\times 10^{-3}$		Cylinder	Anisotropic	Cylinder	Anisotropic
nR1 DB	50.3	—	2500	2105		0.84	
R1 DB	31.7	0.90	2309	2202	2155	0.95	0.93
R2 DB	27.0	4.40	2440	2692	2590	1.10	1.06
nR1 SS	49.6	—	1230	1440		1.17	
R1 SS	31.0	1.70	1496	1627	1530	1.09	1.02
R2 SS	29.0	6.30	1570	1409	1644	0.90	1.05

Note: 1 kN = 0.225 kip.

ASR analysis and shear testing. Perfect bond was assumed between concrete and reinforcement.

The reinforcement properties specified in the analysis were the yield strength, the modulus of elasticity, and the ultimate strength, as summarized in Appendix E. The concrete mechanical property specified was the compressive strength. Two analyses were performed for the reactive specimens depending on the model for the mechanical properties of concrete. In one case, the compressive strength as determined at the test date, from standard 100 mm (4 in.)  $\Phi$  cylinder tests, was used in the analysis. The second analysis employed the proposed anisotropic model for the mechanical properties of concrete in conjunction with the compressive strength of sound concrete at test date. Table 4 summarizes the concrete compressive strengths used in the analyses,  $f_{cp}$ , and the ASR expansion strains considered for the ASR analysis phase  $\epsilon_{ASR}$ . For the anisotropic analyses of the reactive specimens, the compressive strengths measured from the nonreactive specimens nR1 DB and nR1 SS were used.

Shown in Table 4 is a summary of the results presented in terms of shear strength for each test. Note that the ultimate shear strength was reported to be the shear force acting at the midspan of the test region. Both analyses matched well the experimentally measured shear strengths.

The differences between the results obtained using the anisotropic model versus the cylinder properties were negligible for these specimens. One reason behind this was the reinforcement configuration of the beam specimens. The transverse reinforcement provided confinement of the core of the beams, and therefore had a beneficial effect on the overall strength of the specimens. Experimental observations noted that ASR-induced cracks did not penetrate within the structural core of the specimens. It is of interest for future work to analyze the response of ASR-affected beams or slab strips with no transverse reinforcement.

The reactive specimens were found to have a markedly different progression of cracking compared to the nonreactive specimens. The reactive specimens developed diagonal cracks at higher applied shear load and the density of cracks was considerably reduced in comparison to the nonreactive specimens. These test observations are in good agreement with the observations on the behavior of the panel specimens tested as part of this work. Shown in Fig. 9 and 10 are the experimental and analytical crack patterns at failure following the deep beam tests performed on specimens nR1

and R2. The simulated crack patterns match sufficiently well the observed crack patterns, capturing the reduced crack distribution observed for the reactive specimens.

## DISCUSSION AND FUTURE WORK

The proposed model provided reasonably accurate results over the range of conditions examined. However, there are aspects in need of further study.

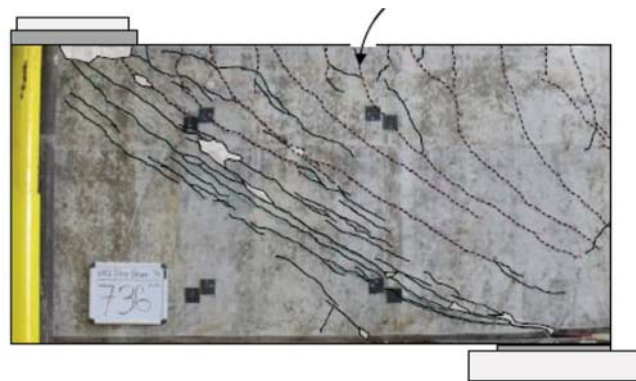
The material-level program that served as a basis for the development of the model investigated a limited set of stress conditions and expansion levels. Additional tests on concrete subjected to long-term multi-axial stresses and undergoing ASR expansion will potentially lead to a more refined model for the mechanical properties of ASR-affected concrete. Additionally, mechanical tests on concrete specimens that have experienced ASR under environmental field conditions would be a valuable addition to the current database. Central to this suggested investigation is the ability to estimate the long-term stress condition.

Data from the literature suggest that ASR-affected concrete exhibits a continuous increase in the Poisson's ratio with the increase of normal stress. This can potentially have a significant influence on the level of confinement induced. The methodology proposed in this study does not address this phenomenon. Future work on this topic could provide further valuable insight on the behavior of ASR-affected structures.

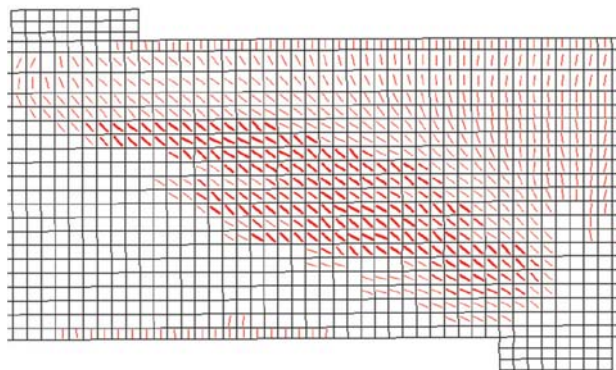
## CONCLUSIONS

The proposed model for the mechanical properties of alkali-silica reaction (ASR)-affected concrete is shown to be a viable approach for modeling reactive shear-critical reinforced concrete elements. There is unequivocal evidence that the concrete mechanical properties are differently affected by ASR-induced damage. Moreover, the deterioration of mechanical properties is direction-dependent. The proposed model, compatible with smeared crack formulations, considers this anisotropy through empirically determined modification factors applied to the compressive strength, modulus of elasticity, and tensile strength of unaffected concrete. The following conclusions are derived from this work:

1. The proposed anisotropic model yields results that closely match experimental observations when used with the Charwood model for ASR expansion. The validation



(a) nR1 DB observed crack pattern at failure



(b) nR1 DB predicted crack pattern at failure

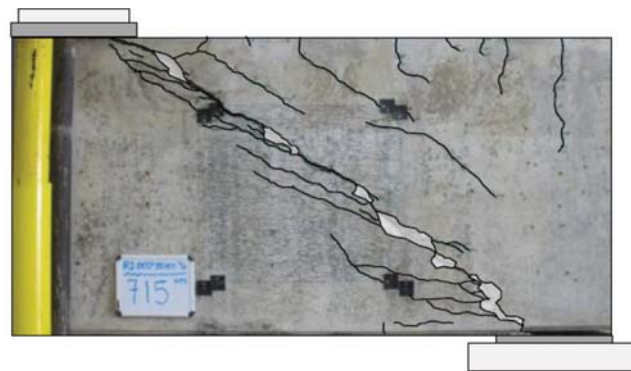
Fig. 9—Nonreactive nR1 DB crack diagrams at failure.

investigation performed on reinforced concrete panels illustrated that the isotropic version of the model produced more conservative results compared to the anisotropic one.

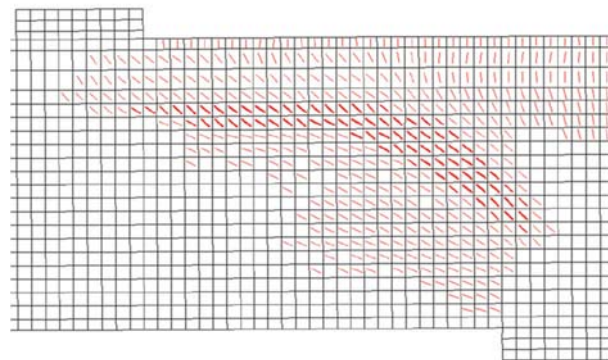
2. The modeling of ASR-affected shear walls produces results that are consistent with the findings obtained from panel specimens. In the shear wall specimens examined, however, the influences were somewhat more muted due to other prevailing mechanisms. The sensitivity study performed for the shear walls revealed that apart from the model for the mechanical properties of ASR-affected concrete, the following mechanisms play an important role in the computed response: ASR expansion effects, modeling of confinement-related mechanisms, and representation of the boundary conditions.

3. In the analyses of shear-critical beams containing at least the minimum shear reinforcement, a significant difference does not exist between the results obtained employing the anisotropic model for the mechanical properties or the isotropic model using the mechanical properties measured on standard cylinder tests. For the beam specimens examined, this was primarily due to the presence of transverse reinforcement that confined the structural core of the beams, and therefore reduced the ASR-induced deterioration.

4. Analyses of shear walls and shear-critical beams reveal no improvement in the accuracy of the computed results when using the more computationally expensive Saouma and Perotti model compared to the much simpler Charwood model.



(a) R2 DB observed crack pattern at failure



(b) R2 DB predicted crack pattern at failure

Fig. 10—Reactive R2 DB crack diagrams at failure.

## AUTHOR BIOS

**Anca C. Ferche** is an Assistant Professor in the Department of Civil, Architectural and Environmental Engineering at The University of Texas at Austin, Austin, TX. She received her PhD from the University of Toronto, Toronto, ON, Canada, in 2020. Her research interests include performance assessment and analysis of reinforced concrete structures, concrete deterioration mechanisms, and rehabilitation of structures.

**Frank J. Vecchio**, FACI, is a Professor in the Department of Civil and Mineral Engineering at the University of Toronto. He is a past member of Joint ACI-ASCE Committees 441, Reinforced Concrete Columns, and 447, Finite Element Analysis of Reinforced Concrete Structures. He has received the ACI Structural Research Award (1998), Structural Engineering Award (1999), Wason Medal for Most Meritorious Paper (2011), Joe W. Kelly Award (2016), and Arthur J. Boase Award (2020). His research interests include advanced constitutive modeling and analysis of reinforced concrete, assessment and rehabilitation of structures, and response to extreme loads.

## ACKNOWLEDGMENTS

The authors would like to acknowledge NSERC for funding support provided to this project. The authors would also like to acknowledge the Ontario Ministry of Transportation and The University of Texas at Austin for providing the reactive aggregate.

## REFERENCES

1. Organisation for Economic Co-operation and Development, *Global Material Resources Outlook to 2060: Economic Drivers and Environmental Consequences*, OECD Publishing, Paris, France, 2019.
2. Ulm, F.-J.; Coussy, O.; Kefei, L.; and Larive, C., "Thermo-Chemo-Mechanics of ASR Expansion in Concrete Structures," *Journal of Engineering Mechanics*, V. 126, No. 3, 2000, pp. 233-242. doi: 10.1061/(ASCE)0733-9399(2000)126:3(233)
3. Grimal, E.; Sellier, A.; Le Pape, Y.; and Bourdarot, E., "Creep, Shrinkage, and Anisotropic Damage in Alkali-Aggregate Reaction Swelling Mechanism – Part I: A Constitutive Model," *ACI Materials Journal*, V. 105, No. 3, May-June 2008, pp. 227-235.
4. Fairbairn, E. M. R.; Ribeiro, F. L. B.; Lopes, L. E.; Toledo-Filho, R. D.; and Silvosio, M. M., "Modelling the Structural Behaviour of a Dam Affected

by Alkali-Silica Reaction,” *Communications in Numerical Methods in Engineering*, V. 22, No. 1, 2006, pp. 1-12. doi: 10.1002/cnm.788

5. Farage, M. C. R.; Alves, J. L. D.; and Fairbairn, E. M. R., “Macroscopic Model of Concrete Subjected to Alkali-Aggregate Reaction,” *Cement and Concrete Research*, V. 34, No. 3, 2004, pp. 495-505. doi: 10.1016/j.cemconres.2003.09.001

6. Esposito, R., and Hendriks, M. A. N., “Literature Review of Modelling Approaches for ASR in Concrete: A New Perspective,” *European Journal of Environmental and Civil Engineering*, V. 23, No. 11, 2019, pp. 1311-1331. doi: 10.1080/19648189.2017.1347068

7. Habibi, F.; Sheikh, S. A.; Vecchio, F. J.; and Panesar, D. K., “Effects of Alkali-Silica Reaction on Concrete Squat Shear Walls,” *ACI Structural Journal*, V. 115, No. 5, Sept. 2018, pp. 1329-1339. doi: 10.14359/51702238

8. NEA/CSNI, “Report on the Phase 2 of the Assessment of Structures Subjected to Concrete Pathologies (ASCET),” *NEA/CSNI/R(2018)4*, Nuclear Energy Agency, Boulogne-Billancourt, France, 2018.

9. NEA/CSNI, “Report on the Phase 3 of the Assessment of Structures Subjected to Concrete Pathologies (ASCET),” *NEA/CSNI/R(2019)11*, Nuclear Energy Agency, Boulogne-Billancourt, France, 2019.

10. Wong, P. S.; Vecchio, F. J.; and Trommels, H., “VecTor2 and FormWorks User’s Manual,” *Technical Report*, Department of Civil Engineering, University of Toronto, Toronto, ON, Canada, 2013, 318 pp.

11. Institution of Structural Engineers (ISE), “Structural Effects of Alkali-Silica Reaction,” SETO, London, UK, 1992.

12. Barbosa, R. A.; Hansen, S. G.; Hansen, K. K.; Hoang, L. C.; and Grell, B., “Influence of Alkali-Silica Reaction and Crack Orientation on the Uniaxial Compressive Strength on Concrete Cores from Slab Bridges,” *Construction and Building Materials*, V. 176, 2018, pp. 440-451. doi: 10.1016/j.conbuildmat.2018.03.096

13. Ahmed, T.; Burley, E.; Rigden, S.; and Abu-Tair, A. I., “The Effect of Alkali Reactivity on the Mechanical Properties of Concrete,” *Construction and Building Materials*, V. 17, No. 2, 2003, pp. 123-144. doi: 10.1016/S0950-0618(02)00009-0

14. Ferche, A. C., and Vecchio, F. J., “Mechanical Properties of Alkali-Silica Reaction-Affected Concrete,” *ACI Materials Journal*, V. 119, No. 1, Jan. 2022, pp. 251-262. doi: 10.14359/51734198

15. VTAG, VecTor Analysis Group, Nonlinear finite element analysis software for reinforced concrete structures, 2019, <http://vectoranalysisgroup.com/>. (last accessed Jan. 27, 2022)

16. Ferche, A. C., and Vecchio, F. J., “Behavior of Alkali-Silica Reaction-Affected Reinforced Concrete Elements Subjected to Shear,” *ACI Structural Journal*, V. 118, No. 4, July 2021, pp. 163-174.

17. Deschenes, D. J.; Bayrak, O.; and Folliard, K. J., “ASR/DEF-Damaged Bent Caps: Shear Tests and Field Implications,” *Technical Report for the Texas Department of Transportation*, 2009, 271 pp.

18. Jurcut, A.-C., “Modelling of Alkali-Aggregate Reaction Effects in Reinforced Concrete Structures,” MASC thesis, University of Toronto, Toronto, ON, Canada, 2015, 136 pp.

19. Ferche, A. C.; Panesar, D. K.; Sheikh, S. A.; and Vecchio, F. J., “Toward Macro-Modeling of Alkali-Silica Reaction-Affected Structures,” *ACI Structural Journal*, V. 114, No. 5, Sept.-Oct. 2017, pp. 1121-1129.

20. Vecchio, F. J., “Disturbed Stress Field Model for Reinforced Concrete: Formulation,” *Journal of Structural Engineering*, ASCE, V. 126, No. 9, 2000, pp. 1070-1077. doi: 10.1061/(ASCE)0733-9445(2000)126:9(1070)

21. Charlwood, R. G.; Solymar, S. V.; and Curtis, D. D., “A Review of Alkali Aggregate Reactions in Hydroelectric Plants and Dams,” *Proceedings of the International Conference of Alkali-Aggregate Reactions in Hydroelectric Plants and Dams*, Fredericton, NB, Canada, 1992.

22. Hobbs, D. W., *Alkali-Silica Reaction in Concrete*, Thomas Telford Ltd., London, UK, 1988.

23. Jensen, A. D.; Chatterji, S.; Christensen, P.; and Thaulow, N., “Studies of Alkali-Silica Reaction — Part II Effect of Air-Entrainment on Expansion,” *Cement and Concrete Research*, V. 14, No. 3, 1984, pp. 311-314. doi: 10.1016/0008-8846(84)90046-2

24. Collins, R. J., and Bareham, P. D., “Alkali-Silica Reaction: Suppression of Expansion Using Porous Aggregate,” *Cement and Concrete Research*, V. 17, No. 1, 1987, pp. 89-96. doi: 10.1016/0008-8846(87)90063-9

25. Beaudoin, J. J.; Feldman, R. F.; and Tumidajski, P. J., “Pore Structure of Hardened Portland Cement Pastes and Its Influence on Properties,” *Advanced Cement Based Materials*, V. 1, No. 5, 1994, pp. 224-236. doi: 10.1016/1065-7355(94)90028-0

26. Bentz, E., “Augustus: Post Processor for VecTor2 (Version 5.8.3),” 2013.

27. Saouma, V., and Perotti, L., “Constitutive Model for Alkali-Aggregate Reactions,” *ACI Materials Journal*, V. 103, No. 3, May-June 2006, pp. 194-202.

28. Barbosa, R. A.; Hansen, S. G.; Hoang, L. C.; and Hansen, K. K., “Residual Shear Strength of a Severely ASR-Damaged Flat Slab Bridge,” *Engineering Structures*, V. 161, 2018, pp. 82-95. doi: 10.1016/j.engstruct.2018.01.056

29. den Uijl, J. A., and Kaptijn, N., “Structural Consequences of ASR: an Example on Shear Capacity,” *HERON*, V. 47, No. 2, 2002, pp. 125-139.

30. Schmidt, J. W.; Hansen, S. G.; Barbosa, R. A.; and Henriksen, A., “Novel Shear Capacity Testing of ASR Damaged Full Scale Concrete Bridge,” *Engineering Structures*, V. 79, 2014, pp. 365-374. doi: 10.1016/j.engstruct.2014.08.027

31. Luo, J. W., “Behaviour and Analysis of Steel Fibre-Reinforced Concrete under Reversed Cyclic Loading,” MASC thesis, University of Toronto, Toronto, ON, Canada, 2014, 315 pp.

32. Carnovale, D. J., “Behaviour and Analysis of Steel and Macro-Synthetic Fibre Reinforced Concrete Subjected to Reversed Cyclic Loading: A Pilot Investigation,” MASC thesis, University of Toronto, Toronto, ON, Canada, 2013, 323 pp.

33. Ferche, A.-C., “Behaviour and Modelling of ASR-Affected Shear-Critical Reinforced Concrete Structures,” PhD dissertation, Department of Civil and Mineral Engineering, University of Toronto, Toronto, ON, Canada, 395 pp.